Characterisation of three-way automotive aftertreatment catalysts and related model systems

S. Bernal*, G. Blanco, J.J. Calvino, J.M. Gatica, J.A. Pérez Omil, and J.M. Pintado

Departamento de Ciencia de los Materiales, Ingeniería Metalúrgica y Química Inorgánica. Facultad de Ciencias, Universidad de Cádiz, Apartado 40, E-11510, Puerto Real (Cádiz), Spain

The techniques applied to the characterisation of three-way automotive aftertreatment catalysts, and some of the most relevant results obtained from those, are briefly overviewed. Studies dealing with both, commercial converters and NM/CeO_2 (CeO_2-ZrO_2) model systems are considered. The analytical and structural characterisation studies on commercial TWCs reported here are mainly devoted to the identification of some of the most relevant factors causing their deactivation. Regarding the reviewed literature on model systems, some more fundamental aspects are considered. Among them, the use of HRTEM, spectroscopic, and chemical techniques in studies on metal sintering and re-dispersion, metal/support interaction phenomena, and redox characterisation of ceria-based catalytic materials are discussed.

KEY WORDS: TWC; characterisation techniques; deactivation; poisoning effects; thermal ageing; metal sintering; strong metal/support interaction effects; OSC behaviour

1. Introduction

The very first automotive aftertreatment devices simply consisted of Pt-Pd/Al_2O_3 oxidation catalysts [1]. A significant reduction of the CO and unburned hydrocarbon emissions could be achieved with them. However, in 1981, stricter exhaust standards, particularly for nitrogen oxides, were introduced in the US legislation on passenger car emissions [2]. Profound modifications had to be introduced in the design of the catalytic converters. The solution to this very challenging problem came from a collaborative research effort of different industrial sectors. Parallel developments in gasoline formulation, engine management and control systems, and of course in catalyst design were necessary. A revolutionary concept, the three-way catalysis (TWC), implying the simultaneous conversion of the three major pollutants, CO and hydrocarbons (oxidation), and NO_x (reduction), was introduced [2].

In addition to Pt, Rh was incorporated to the catalyst because of its high activity in NO_x reduction [1,3,4]. Likewise, in order to ensure a high conversion of all the pollutants, it became critically important to keep the redox balance of the exhaust mixture, i.e., its air-to-fuel (A/F) ratio, as close as possible to the stoichiometric point, A/F = 14.7 [5]. To achieve this, ceria, an oxygen storage component attenuating the A/F oscillations, was added to the catalyst formulation [1]. Accordingly, by the second half of the 1980s, a typical three-way catalyst consisted of a cordierite (ceramic) honeycomb substrate [6–8], and a few tens micron thick washcoat [6,9,10] containing γ-Al_2O_3, as a carrier [5], noble metals, mainly Pt/Rh in ratio of around 5:1 [11], ceria, as oxygen buffer material [12], and some alumina stabilisers like lanthana, silica, or baria [5,13].

Presently, TWC is an essential component of the emission control system of all the spark-ignited motor vehicles commercialised in the US, the EU, Japan, and many other countries [13,14]. As a number of authors have recently stressed [4–6], the development of TWCs represents one of the greatest successes of the environmental protection technologies, and also of the recent history of heterogeneous catalysis.

Though the main principles governing the design of TWCs have remained over the years, significant modifications have been progressively introduced in both their formulation and the component distribution in the converter [14]. Increasingly demanding emission standards [6,14] and durability requirements [6], as well as the reduction of catalyst costs [6,14,15] have been some of the major driving forces for these successive modifications.

Regarding the noble metals, the incorporation of Pd to the TWC formulations is particularly noticeable. The gradual reduction of sulfur and the residual lead levels in unleaded gasolines opened the door for partial or complete substitution of Pt by Pd in the classic Pt/Rh formulation [10,14]. Currently, Pt/Rh, Pt/Pd/Rh, Pd/Rh, and Pd-only TWCs are commercialised [4]. Improvements in OSC materials have also been very

* To whom correspondence should be addressed.
E-mail: serafin.bernal@uca.es

1022-5528/04/0400–0031/0 © 2004 Plenum Publishing Corporation

remarkable, the introduction in the mid 1990s of ceria–zirconia representing a major breakthrough point [5,12,16]. Compared to bare ceria, CeO_2–ZrO_2 mixed oxides show better textural stability [17,18], enhanced redox activity [18], and better resistance to the chemical (redox) deactivation upon thermal ageing [18].

For certain specific applications, metallic monoliths are also being used. These monoliths, typically consisting of stainless steel alloys, allow a reduction in the converter volume without loss of efficiency [6]. Better adherence of the catalyst coating, and considerably higher thermal conductivity have also been considered as advantages of the metallic monoliths [10].

The washcoat technology has become more and more sophisticated. Deploying the noble metals in different washcoat layers, or even on different support phases within the same layer, have contributed not only to the prevention of undesirable deactivation effects [13], but also to the optimisation of the catalyst [14]. Accordingly, layered washcoating is a common practice in current TWC technology [6,14]. Preparation methods allowing control of the axial distribution of components have also been developed. Such is the case of the zone coating technology, currently used for segregating the different noble metals along the monolith channels. In this way, deactivation effects due to alloying phenomena are prevented [14].

The car emission regulations enacted in the 1990s, and particularly the LEV, ULEV and SULEV standards in California, put special emphasis on the control of the hydrocarbon emissions. The majority of these emissions (60–80%) take place during the first 2 min after ignition of the engine [6]. The technologies developed to control these cold start emissions have recently been discussed [5,6,13]. The combination of a catalyst mounted in the close vicinity of the engine exhaust ports (Close coupled catalyst), with an underfloor converter has been considered one of the best options [6]. The close coupled catalyst, specifically designed for sustainable performance after aging at 1323 K, would mainly convert the hydrocarbons, whereas, the underflow catalyst should remove CO and NO_x [6]. Different formulations are obviously required for these two catalysts [6].

In recent years, the introduction of gasoline lean burn engines has represented a new challenge for the designers of automotive converters [19]. The combination of a NO_x trap system and the three-way catalyst seems to be the most promising alternative [5,6,20]. Under net oxidising conditions, the TWC is effective for CO and HC oxidation, but not for lean NO_x reduction [6]. Consequently, a catalytic trap consisting of Pt/BaO/Al_2O_3 ought to be incorporated to the aftertreatment device [5,6]. During the lean operation period (60 s), NO is catalytically oxidised to NO_2 over Pt, and stored on baria; after this time, the engine operates for less than 1 s in fuel rich mode, thus triggering the desorption of NO_x, which is then reduced to N_2 on the TWC [6,21].

Because of the extraordinary scientific, technological and economic relevance of the automotive aftertreatment technologies, a great research effort has been devoted to their development. An important part of this effort has been focused on different aspects of the catalyst characterisation. As deduced from the considerations above, however, the increasing complexity of these catalytic devices, even if limited to those used in gasoline-fuelled vehicles, makes a comprehensive overview of the characterisation problems found in all of them very challenging. Accordingly, this review will be specifically devoted to the studies dealing with three-way catalysts, the most representative of the in-use technology for the abatement of emissions from spark-ignited automobiles. The characterisation of both fresh and aged TWCs will be considered. Studies on model systems will also be discussed. Because of the limitations imposed by the complexity of commercial converters, the investigation on model catalysts has provided extremely useful information about the role played by the different components in real converters, their interactions, and the mechanisms involved in their deactivation. Likewise, the studies on model systems have contributed to the design of specific methodologies which eventually might be applied to the characterisation of TWCs.

2. Characterisation studies on commercial TWCs

Most of the reported characterisation studies on commercial TWC converters have been devoted to the investigation of the major factors causing their deactivation. The identification of these factors, the evaluation of their specific relevance, and their way of action have constituted the main goals of these studies. The usual experimental approach has consisted of the parallel investigation of fresh and aged catalysts, the determination of the changes occurred upon ageing, and, eventually, the analysis of the relationship existing between the observed modifications and the chemical (redox) [22,23] and catalytic [22,24,25] behaviour. As will be briefly commented on below, a relatively limited number of experimental techniques have been used in these studies. The complex structure of commercial converters, and the low content of some of their key components, particularly the noble metals, constitute some of the major reasons explaining the difficulty of more detailed characterisation studies.

As discussed in [9,26,27] there are a number of well identified factors causing catalyst deactivation: poisoning, fouling, thermal degradation, vapour compound formation accompanied by transport, and mechanical degradation (attrition/crushing). All these factors have been considered to play a more or less relevant role in the case of TWCs.

2.1. Analytical characterisation studies on commercial TWCs

Figure 1 shows a commercial TWC converter and a SEM image that identifies the ceramic monolith and the thin washcoat covering its inner walls.

In some cases, the analytical studies are carried out on small pieces of the brick, including both the monolith and the washcoat [22,25,28,29]. Samples are typically obtained by cutting the brick axially and transversally with the help of an appropriate saw. In this way analytical determinations could be made in selected well defined regions of the converter [28]. In some other cases, the monolith/washcoat pieces are further ground and sieved before analysing them [22,25,29].

In addition to wet techniques, scanning electron microscopy-energy dispersive spectroscopy SEM-EDS [9,22], electron probe micro-analysis (EPMA), X-ray fluorescence (XRF) [22,25,29], Laser-induced breakdown spectrometry (LIBS) [30], and Particle-Induced X-ray emission (PIXE) [28,31], are some of the techniques used in these analytical studies. Further details about the advantages and limitations of the techniques above may be found in the related literature.

Table 1 summarises some results of an XRF study carried out on a catalyst which has been aged under real driving conditions, and the corresponding fresh sample. The results account for the changes observed in the main contaminant elements. No data for the well known components of the TWCs (NMs, alumina and ceria–zirconia) are reported.

The results in table 1 are in good qualitative agreement with several other analytical studies on aged catalysts [9,25,28,29]. In accordance with these, P, Zn, Ca, and Pb, are some of the most typical contaminants in aged TWCs. The first three elements are generated by combustion in the engine of lubricant additives [9,22–24,29], whereas the fourth one would come from fuels that still contain significant amounts of lead. Though not included in table 1, sulfur, from the fuel, has also been reported as a contaminant often detected in aged catalysts [9,23].

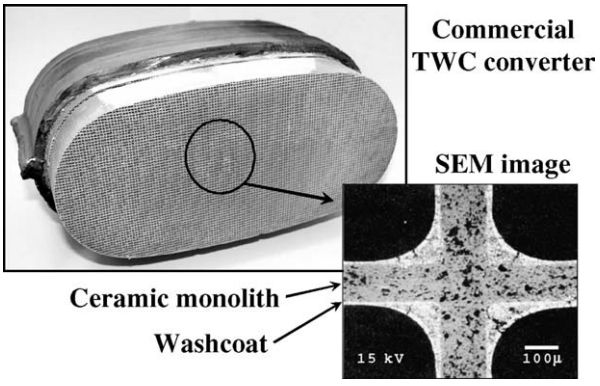

Figure 1. Commercial TWC converter. Detail of the washcoat as revealed by SEM (scanning electron microscopy).

Table 1
Total reflection X-ray fluorescence analysis of the main contaminant elements present in an aged TWC converter [22]

Element	Fresh sample[a]	Aged sample[a]
Si[b]	100 ± 1	100 ± 1
P	0.15 ± 0.03	3.9 ± 0.7
Ca	0.71 ± 0.05	1.09 ± 0.08
Zn	0.093 ± 0.001	0.41 ± 0.01
Pb	0.034 ± 0.001	0.42 ± 0.02
Cr	0.10 ± 0.01	0.17 ± 0.02
Cd	not detected	0.17 ± 0.02
Cu	0.041 ± 0.002	0.091 ± 0.004
Ni	0.020 ± 0.002	0.053 ± 0.01

Data for both the fresh and aged samples are mass-referred to Si = 100.

[a]Studies performed on the very first millimetres of the front monolith mounted in a Ford Focus 2.0 (1999 model). The converter was aged under real driving conditions for 30.000 Km.

[b]Element used as reference. It is a major component of the cordierite monolith ($5SiO_2{\cdot}2Al_2O_3{\cdot}2MgO$) [22].

Compared to the thickness of the washcoat, 20–30 μm [6,9,10], the resolution of SEM–EDS (1 μm) allows the application of this techniques in analytical studies of the radial distribution of elements in both fresh and aged samples [22]. In this way, a rough estimate of the compositional profile in layered washcoats may be obtained [6]. Likewise, this sort of technique has been used for gaining information about the radial distribution of contaminants [22,25]. Studies aimed at evaluating the loss of noble metals occurred by volatilisation and incorporation into the exhaust stream are also available [30].

The analytical studies briefly commented on above have also contributed to the development of routines for regenerating aged TWCs [9,24]. By determining the composition of aged catalysts before and after applying a certain regeneration treatment, its specific effects could be evaluated. Moreover, testing the catalytic behaviour of regenerated samples has allowed us to gain information about the relative influence of poisoning and thermal ageing phenomena on the catalyst deactivation [24].

2.2. Structural characterisation studies on commercial TWCs

X-ray diffraction (XRD) is by far the most commonly used technique in structural characterisation of commercial TWCs [22,25,28,31]. Valuable information has been obtained from these studies. In aged catalysts, XRD studies have allowed the identification of the crystalline phases formed by the contaminants deposited on them. Thus, considerable information has been gained about the structural nature of the phosphorus-containing contaminants in poisoned automotive catalysts [22,25,28,31]. In accordance with these studies,

phosphorus is mainly present in the form of a variety of phosphates phases. The analysis of their characteristic peaks in the XRD patterns has allowed the identification of $MgZn_2(PO_4)_2$ [25], $CaZn_2(PO_4)_2$ [25], and $CePO_4$ [22,28]. In [22], the formation of $CePO_4$ is considered to be the main factor responsible for the loss of OSC observed in the aged catalyst as compared to that determined for the fresh one. Phosphorus may also be present as amorphous or very poorly crystallised phases [25]. In this case, an alternative technique, MAS–NMR of ^{27}Al and ^{31}P, has shown the presence of $AlPO_4$ and $Zn_3(PO_4)_2$ in the aged catalysts [25].

Other phases detected in XRD studies of aged TWCs are $CeAlO_3$, cerium aluminate, and $CeBa_{0.13}Mg_{0.87}Al_{11}O_{17}$, cerium barium magnesium hexa-aluminate [28,31]. Both are known to be formed at high temperature, under reducing conditions, and to cause deactivation of the OSC material because of the stabilisation of the Ce(III) oxidation state. Particularly noticeable is the observation of the latter phase. As discussed in Refs. [28,31], in which converters using CeO_2 as OSC material are studied, the presence of Mg in the hexa-aluminate phase requires the participation of the cordierite monolith in the process. The authors conclude that their observation can only be explained assuming a prolonged exposure of the converter, at very high temperature (≥1373 K), under rich operation conditions.

XRD has also been used for detecting thermal ageing phenomena in TWCs used under real driving conditions. A typical manifestation of these phenomena is the occurrence of significant sintering/micro-crystal growth in both the OSC materials and the noble metal phases. Narrowing of their characteristic diffraction peaks, which is considered to be an experimental indication of such effects, has been reported for ceria [28] and ceria zirconia [22] in XRD studies of aged TWCs. In spite of the low noble metal content of commercial TWCs, typically not exceeding 0.5 wt% of washcoat [28], evidence of thermal ageing effects could also be obtained from the analysis of XRD peaks for Pd [22]. The detection of characteristic diffraction peaks of α-Al_2O_3 [31], which is typically formed by the virtue of the γ-$Al_2O_3 \rightarrow \alpha$-$Al_2O_3$ phase transition, may also be used as an indication of significant thermal ageing in TWCs.

3. Characterisation studies on TWC model systems

In recent years numerous review works have been devoted to the characterisation of the chemical, textural and nano-structural properties of ceria-based catalytic materials [16,32–35]. Most of these studies have dealt with ceria, ceria–zirconia mixed oxides, and the corresponding NM (Rh, Pd, Pt)/CeO_2 (CeO_2–ZrO_2) catalysts, thus indicating their close relationship with fundamental research on three-way catalysis. Here, we shall consider some major aspects of the characterisation of these materials. Findings reported in some recent work not included in the above mentioned reviews, will also be considered.

3.1. Characterisation studies of noble metal phases supported on ceria and ceria–zirconia mixed oxides

3.1.1. Nano-structural characterisation of the supported noble metal phases

High resolution transmission electron microscopy (HRTEM) studies have played a very relevant role in the nanostructural characterisation of noble metal (NM) phases highly dispersed on CeO_2 and CeO_2–ZrO_2 supports [36,37]. A number of contributions of HRTEM should be outlined.

In accordance with the computer simulation HRTEM imaging studies reported in [38,39], f.c.c. noble metal nano-crystals supported on ceria typically consist of truncated cube-octahedron particles. Likewise, the criteria for determining the metal nano-crystal size, and the detection limit (1 nm) have been established [38,39]. On the bases of these studies, the statistical analysis of HRTEM micrographs corresponding to NM/CeO_2 (CeO_2–ZrO_2) catalysts has allowed us to determine the NM particle size distribution in a variety of catalysts belonging to this family of model systems. An example of these studies is reported in figure 2.

The availability of meaningful metal particle size distributions for a variety of NM/CeO_2 (CeO_2–ZrO_2) catalysts has been crucial for gaining some further information about a number of very challenging characterisation problems found in these model systems.

If mathematically treated in an appropriate manner [38], particle size distributions may provide reliable metal dispersion data. Accordingly, HRTEM has been very fruitfully used in studies of metal sintering behaviour of NM/CeO_2 and closely related catalysts under a wide variety of thermal ageing treatments, including both reducing and oxidising conditions. Some examples of these studies may be found in Refs. [36,37,40,41]. Figure 3 reports on the evolution of normalised, HRTEM metal dispersion data, i.e., $[D_{HRTEM}(T_{red} = T\ K)]/D_{HRTEM}\ (T_{red} = 623\ K)]$, for a number of Rh(Pt)/CeO_2 ($Ce_{0.68}Zr_{0.32}O_2$) catalysts reduced at temperatures ranging from 623 to 1173 K. Though the surface density of both Rh and Pt is approximately 20 times smaller in the ceria–zirconia catalysts, parallel trends are observed on both, CeO_2- and $Ce_{0.68}Zr_{0.32}O_2$-supported systems, thus suggesting that, under reduction conditions, rhodium exhibits a higher resistance against sintering than platinum.

HRTEM metal dispersion data are free from the uncertainties of the classic chemisorption studies at 298 K (see section 3.1.2 below). Accordingly, they may be used as reference values for the volumetric studies. In

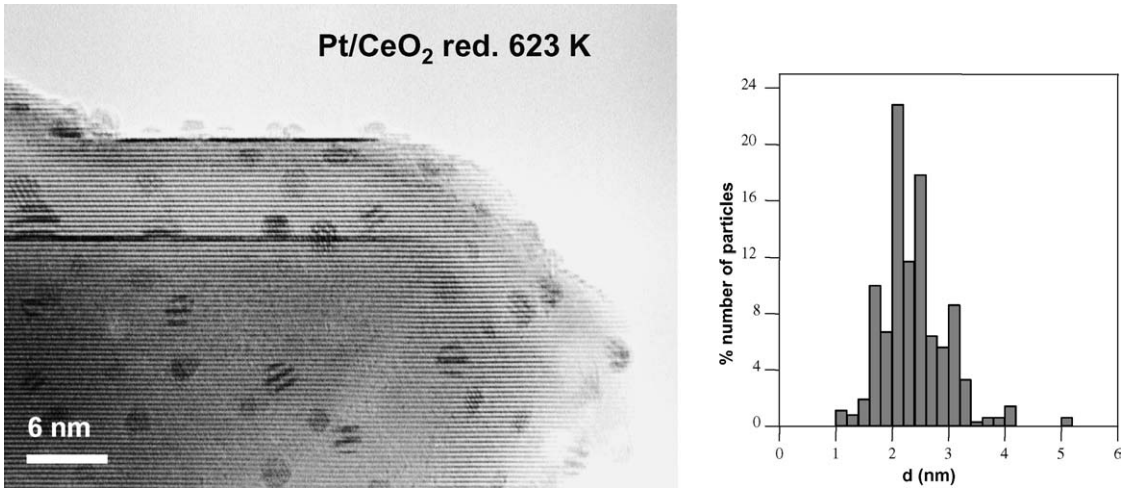

Figure 2. HRTEM study of the metal dispersion in $NM/CeO_2(CeO_2–ZrO_2)$ catalysts. Examples of experimental HRTEM image and of metal nano-crystal size distribution resulting from the analysis of series of micrographs like the one shown here. Catalyst: Pt/CeO_2 reduced at 623 K.

fact, the combination of HRTEM and volumetric techniques has been fruitfully used for developing a specific hydrogen chemisorption routine providing reliable metal dispersion values for $Rh(Pt)/CeO_2(CeO_2–ZrO_2)$ catalysts [36,40,41].

Other nano-structural features of NM/CeO_2 (ceria-based mixed oxides) catalysts which have been well characterised by means of HRTEM, are those related to what generically may be referred to as metal/support interaction phenomena.

Epitaxial growth of the noble metal particles (Rh, Pt, and Pd) supported on ceria [36,39,42–45], ceria–zirconia [40,41], and some other ceria-based supports [37], has been systematically observed over the whole range of the investigated reduction temperatures. It is therefore a very general characteristic feature of all these catalysts. Two different types of metal/support structural relationships are presently well characterised [37]. Examples of these are shown in figure 4.

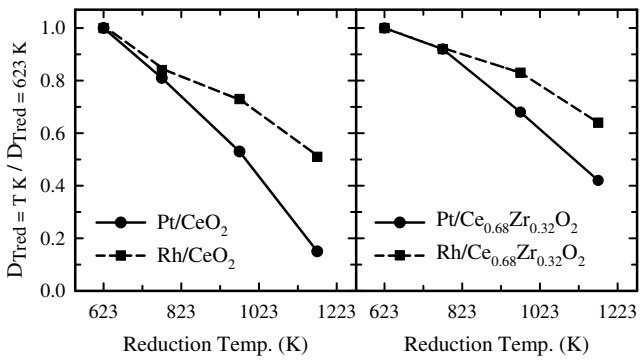

Figure 3. Effect of the reduction temperature on the normalised HRTEM metal dispersion data, [D_{HRTEM} (T_{red} = T K)/D_{HRTEM} (T_{red} = 623 K)], for a series CeO_2- and $Ce_{0.68}Zr_{0.32}O_2$-supported Rh and Pt catalysts.

The occurrence of metal decoration effects is presently well established on ceria-based catalysts. Figure 5 shows an example of a noble metal particle covered by a very thin layer of the reduced ceria support.

On $Rh(Pt)/CeO_2$ catalysts, reduction treatments with hydrogen at $T \geq 973$ K are typically required for inducing partial or even total covering of the metal nanocrystals [36,46,47]. A remarkable difference may be noted between ceria- and ceria–zirconia mixed oxide-supported catalysts. In the latter case, decoration effects could only be observed on Rh [40] and Pt [41] catalysts

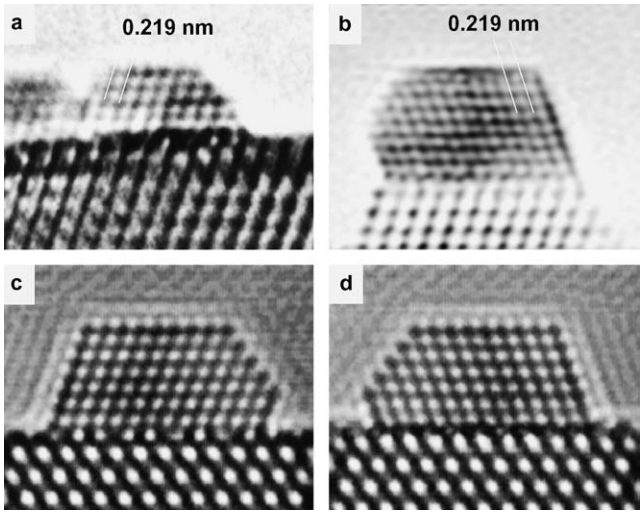

Figure 4. Metal/support structural relationships in NM/CeO_2 and closely related model catalysts: (a) HRTEM experimental image of a Rh/CeO_2 catalyst reduced at 773 K. Metal and support crystallographic axes are all aligned, (b) experimental image of a Pt/CeO_2 catalyst reduced at 773 K. Metal/support interface consists of (111) planes in parallel orientation; other metal crystallographic axes are rotated 60° with respect to those of the support, (c) and (d) computer simulated HRTEM images supporting the interpretation of the experimental micrographs shown respectively in (a) and (b).

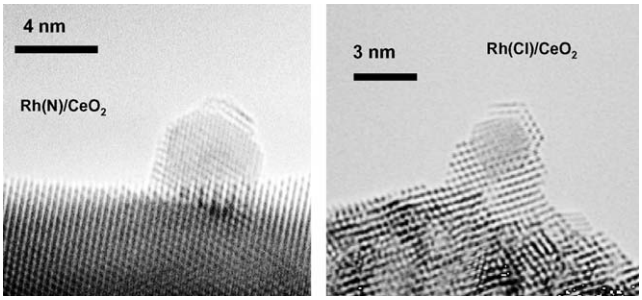

Figure 5. HRTEM images illustrating the decoration phenomena observed in ceria-supported noble metal and some closely related model catalysts. Micrographs corresponding to: (a) $Rh(N)/CeO_2$ reduced at 1173 K. Sample prepared from $Rh(NO_3)_3$, (b) $Rh(Cl)/CeO_2$ reduced at 973 K. Sample prepared from $RhCl_3$.

reduced at 1173 K, the fraction of covered particles not exceeding 5% of the total metal crystallites [40]. Though $(5\%)H_2/Ar$, instead of pure H_2, was used in the reduction treatments [40,41], this observation suggests that, compared with bare ceria, the reduced ceria–zirconia mixed oxides either exhibit a lower surface mobility or its interaction with the metal particles is weaker. Since the sintering behaviour of Rh and Pt is similar on both ceria and ceria–zirconia supports [37], the differences noted in the intensity of the decoration effects is more likely due to the different surface mobility of the reduced oxides (CeO_{2-x} or $Ce_yZr_{1-y}O_{2-x}$).

HRTEM and X-ray diffraction studies on Pt/CeO_2 [46] and Pd/CeO_2 [43,48] have shown the occurrence of Ce–NM alloying phenomena. No similar effect has ever been detected in Rh/CeO_2 [36]. Regarding the Pt/CeO_2 catalysts, alloying could only be observed upon reduction at $T \geq 1173$ K [46]. A well defined inter-metallic phase, $CePt_5$, has been unequivocally identified by combined analysis of the experimental and computer-simulated images [46].

The incorporation of Ce into the Pd micro-crystals has been observed by reduction of Pd/CeO_2 catalysts at temperatures as low as 773 K [48]. In contrast to that found in Pt/CeO_2, no HRTEM or XRD evidence of stoichiometrically well defined inter-metallic Ce-Pd phases could be obtained, even in catalyst samples reduced for 20 h at 1180 K [43]. Accordingly, a Ce–Pd solid solution, iso-structural with the f.c.c. metallic palladium, is proposed to be formed [43,48]. The experimental basis for such a proposal is the shift observed in the position of the X-ray diffraction peaks for metallic Pd. This shift is interpreted as due to the slightly larger (2.3%) lattice parameter of the Ce–Pd solid solution.

No alloying phenomena have been reported on NM/CeO_2–ZrO_2 catalysts as yet. This suggests that, as in the case of decoration effects, the incorporation of zirconia into the ceria lattice stabilises the support against the solid state reaction leading to the formation of Ce–NM alloys.

Though metal decoration or alloying phenomena are seldom considered as a deactivation factor in commercial TWCs, characterisation studies carried out on converters aged under real working conditions have shown the likely occurrence of prolonged overheating effects ($T \geq 1373$ K) under net reducing conditions [28]. This effect, though probably due to a failure in the electronic control of the engine, does certainly create thermo-chemical conditions under which the occurrence of the above mentioned phenomena cannot be disregarded.

HRTEM has also been systematically applied to the investigation of the nano-structural evolution undergone by ceria-supported Rh and Pt catalysts heated under oxygen at temperatures ranging from 373 to 1173 K [36,37,49]. These studies had two major goals: (a) to establish the experimental re-oxidation conditions allowing the recovery of the catalysts from decorated or alloyed states; and (b) to investigate the effect on the metal dispersion of the oxidising treatments.

Regarding the reversion of the decorated or alloyed effects, HRTEM combined with electron energy loss spectroscopy (EELS) studies has clearly shown that re-oxidation treatments at temperatures well above 773 K are required [37,50]. This is a remarkable observation, because, as discussed in [36], 773 K is a typical re-oxidation temperature for regenerating catalysts from the SMSI (strong metal–support interaction) state.

As far as the effect of the oxidising treatments on the metal dispersion is concerned, the results of the SEM-EDS study reported in [36] suggest the existence of significant differences between Rh and Pt. The differences are particularly noticeable between the catalysts heated under flowing oxygen at 1173 K. This treatment induces re-dispersion of Rh, whereas in the case of Pt a strong bimodal distribution consisting of small metal nano-crystals (2–3 nm) coexisting with a fraction of much bigger particles (1 μm) is observed. The nano-structural constitution of the oxidised Rh and Pt particles is also different. Over a wide range of oxidation temperatures (623–1173 K), rhodium particles consist of Rh_2O_3 [36]. By contrast, no evidence of any well defined platinum oxide could be deduced from the HRTEM images corresponding to catalysts treated in the same way as those of Rh [36]. In the case of Pt, accordingly, the different treatments would only affect the outer layers, a nucleus of reduced Pt being always present in the particles.

3.1.2. *Chemical characterisation of the supported noble metal phases. H_2 and CO chemisorption studies*

Numerous volumetric data for both H_2 and CO chemisorption on NM/CeO_2 (CeO_2–ZrO_2) catalysts have been recently reported [37]. These data are typically used for determining metal dispersions, but also for detecting the metal deactivation effects due to the occurrence of an SMSI effect [41].

As already discussed [37], however, the interpretation of volumetric chemisorption data for ceria-based model catalysts, often recorded at 298 K, is complicated by a number of side effects which should be carefully controlled in order to arrive at meaningful conclusions. Among others [36], the likely occurrence of simultaneous chemisorption of the typical probe molecules (H_2 and CO) on both metal and support is acknowledged to be a major restriction to the straightforward use of volumetric data in estimates of the metal dispersion [35,36]. The likely occurrence of strong metal support interaction (SMSI) effects may also disturb the correlation between H(CO)/NM and metal dispersion data.

Establishing the occurrence of a true SMSI effect in $NM/CeO_2(CeO_2–ZrO_2)$ catalysts also requires a careful analysis of the chemisorption data. Contributions to the eventual loss of chemisorption capability of factors other than the metal deactivation, such as metal sintering or metal encapsulation (support sintering), particularly important in high surface area catalysts, should be excluded, or at least quantitatively evaluated [36].

To summarise, the use of H_2 (CO) chemisorption data for determining metal dispersions or detecting the existence of SMSI effects in NM/CeO_2 ($CeO_2–ZrO_2$) catalysts is strongly limited by a number of side effects. Additional characterisation data are therefore necessary in order to arrive at meaningful conclusions. Some examples of fruitful combination of chemisorption studies and several other characterisation techniques, particularly HRTEM, will be commented upon below.

3.1.2.1. Hydrogen chemisorption studies

It is presently well established that, under the usual experimental conditions of volumetric chemisorption studies, strong hydrogen spillover phenomena may occur in NM (Rh, Pd, Pt)/CeO_2 ($CeO_2–ZrO_2$) catalysts. Numerous Faraday magnetic balance studies have unequivocally shown the occurrence of such an effect [51–55]. Likewise, studies of the time required to reach an apparent equilibrium in volumetric studies, at 298 K, carried out on $NM/CeO_2–ZrO_2$ catalysts support the existence of spillover effects [40,41]. Thus, if spillover significantly contributes to the total amount of chemisorbed hydrogen, the equilibrium times may be more than 15 times longer than in the absence of it [40]. Apparent H/NM values $\gg 1$ [40,41,56] would also constitute a clear indication of the occurrence of spillover effects.

Low temperature chemisorption experiments, at 191 K, have been shown to be a useful way of minimising the hydrogen spillover contribution in NM/CeO_2 ($CeO_2–ZrO_2$) catalysts [36,40,41,56–58], thus providing H/NM values which might be used for estimating the metal dispersion. This proposal has been fully confirmed by parallel HRTEM studies in Rh and Pt catalysts [36,40,41]. In the case of supported Pd systems there are still difficulties because of the formation of bulk hydrides. Although studies aimed at simultaneously controlling the spillover and bulk hydride contributions have been carried out on Pd/$CeO_2–ZrO_2$, no reliable experimental protocol has been established as yet [41].

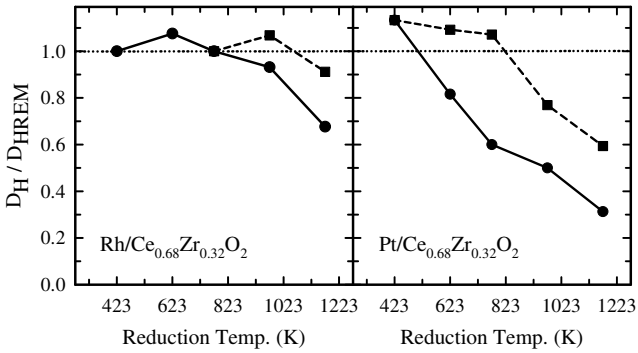

Figure 6. Metal deactivation effects in $Rh(Pt)/Ce_{0.68}Zr_{0.32}O_2$ catalysts as revealed by the combined application of low temperature (191 K) hydrogen chemisorption (D_H) and HRTEM (D_{HRTEM}) studies. Catalysts reduced for 1 h, under flowing H_2(5%)/Ar. (■) Catalysts reduced at the indicated temperature, further re-oxidised at 700 K, and finally reduced at 423 K. Data taken from [40,41].

The combination of low temperature volumetric experiments and HRTEM studies has also been fruitfully applied to the characterisation of the SMSI effects occurring in some of these model catalysts [40,41]. Figure 6 summarises the results of parallel studies carried out on $Rh(Pt)/Ce_{0.68}Zr_{0.32}O_2$ reduced at temperatures ranging from 423 to 1173 K. In this figure, the evolution of the D_H/D_{HRTEM} ($D_H = H/NM$, i.e., the metal dispersion as determined from hydrogen chemisorption at 191 K; D_{HRTEM} = Metal dispersion as determined from HRTEM studies) against T_{redn} is plotted. Metal encapsulation effects are excluded because of the high textural stability of the oxide support [40,41]. Accordingly, in the absence of SMSI effect, D_H/D_{HRTEM} should be equal to 1, $D_H/D_{HRTEM} < 1$ showing the onset of metal deactivation phenomena.

In accordance with figure 6, the loss of chemisorption capability varied remarkably from one noble metal to the other, Rh being less sensitive than Pt to the increase of the reduction temperature. The Pd behaviour resembles that of Pt [41].

The results above suggest that reduction temperatures below 573 K should be applied in order to obtain meaningful metal dispersion data from hydrogen chemisorption studies. It is also worth noting that the deactivation effect may be totally or partially reversed upon re-oxidation at 700 K and further reduction at 423 K. As discussed in Refs [40,41], the observed metal deactivation is mainly due to electronic effects, with no significant contribution of the metal decoration or alloying phenomena.

^{1}H-NMR technique has also been fruitfully applied to the investigation of the hydrogen adsorption on ceria-

supported noble metal catalysts [59]. Because of the different chemical shift shown by the hydrogen species chemisorbed on the metal and the ceria support, the evolution of the rhodium chemisorptive capability as a function of T_{red} could be studied. In [59] Rh/CeO_2 catalysts prepared from both chloride (Cl) and nitrate (N) metal precursors were investigated. Upon increasing the reduction temperature, metal deactivation effects are observed on both, the effect being stronger in the case of the (N) sample. Re-oxidation at 673 K of the pre-reduced catalysts allows recovery from the deactivated state [59].

3.1.2.2. CO chemisorption studies

As deduced from the volumetric chemisorption data reported in [37], CO has also been widely used as a probe molecule for characterising ceria-supported noble metal catalysts. This technique has also been used for estimating metal dispersions in real TWC washcoats [10].

It should be stressed, however, that there are a number of factors which may very much disturb the relationship existing between the experimental CO/NM ratios and the true metal dispersion. In addition to the problems inherent to the CO–NM stoichiometric ratio, it is known that CO may be strongly interact with ceria-based supports [60–65]. Moreover, the amount of chemisorbed CO very much depends on variables like the support redox state [60,63], or its chloride content [66,67]. In this latter respect, it is worth recalling that large amounts of Cl^- may be incorporated into the ceria lattice when catalysts are prepared from chlorine-containing NM precursors [37].

FTIR spectroscopy allows us to distinguish CO species chemisorbed on the NM and the ceria-based supports, thus circumventing the problems of volumetric techniques mentioned above. Consequently, it has also been applied to the determination of metal dispersion in NM/CeO_2 catalysts [62]. By using appropriate calibration data, the integrated absorption of the recorded CO–NM bands could be correlated with the number of surface metal atoms, and therefore, provided that the total number of metal atoms in the catalyst is known, with the metal dispersion. This approach has been used for estimating metal dispersions in Pt/CeO_2 [62] and Pd/CeO_2 [68] catalysts.

Another method allowing us to subtract the support contribution from the total amount of CO chemisorbed on Pt/CeO_2 has been reported in [69]. The authors claim its usefulness for determining true metal dispersion data.

Upon increasing the reduction temperature, a progressive loss of the metal chemisorption capability for CO has been reported to occur on Pt/CeO_2 [61,62,70,71], Pd/CeO_2 [63,64,72], and Rh/CeO_2 [65] catalysts. The effect typically consists of a partial rather than total deactivation of the metal. As deduced from the results reported in [70] for a Pt/CeO_2 catalysts reduced at 773 K, very mild re-oxidation treatments, either with O_2 at 298 K, or even with CO_2 at 473 K, allow significant recovery of the CO chemisorption capability of the deactivated catalyst.

As already noted for hydrogen, the use of CO adsorption in metal dispersion studies requires a careful selection of the reduction temperature. The available information suggests that $T_{red} \leq 573$ K may be appropriate for preventing the induction of significant metal deactivation effects [36,41,70].

3.2.Characterisation studies on the OSC materials

Redox materials for TWC applications must fit very demanding kinetic and thermodynamic requirements. They should be able to rapidly release/uptake as much oxygen as possible, within a wide range of operation temperatures. Likewise, they should show a high stability against thermal deactivation under varying redox conditions. Accordingly a great effort has been devoted to characterising and better understanding these properties.

A very wide battery of experimental techniques have been applied to the redox characterisation of ceria and ceria-based mixed oxides. Among them are, temperature-programmed-reduction (TPR) [37,73–86], -oxidation (TPO) [87,88], oxygen (hydrogen, CO) pulse techniques, usually applied in oxygen storage capacity (OSC) and oxygen buffering capacity (OBC) experiments, to be commented on below, Faraday magnetic balance [37,51,55,77,86,89–96], X-ray absorption near edge spectroscopy (XANES) [55,97–101], electron energy loss spectroscopy (EELS) [97,102–104], X-ray photo-electron spectroscopy (XPS) [97,99, 101,105–116], electron paramagnetic resonance (EPR) [99,117–121], FTIR of appropriate chemisorbed probe molecules [87,122–126], and electronic conductivity measurements [127,128], are some of the most commonly applied techniques.

A few major conclusions from these studies should be outlined here. When heated under hydrogen, ceria [37,53] and ceria–zirconia [55] may undergo two different reduction processes. The first one, which is referred to as reversible [53], is associated with hydrogen chemisorbed on the oxide. Its contribution to the total reduction degree is particularly important in high surface area NM/CeO_2 (CeO_2–ZrO_2) catalysts [37,53,55] reduced at or below 623 K. Spillover effects play a key role. A further characteristic is that this reduction process may be reversed by evacuation of the chemisorbed hydrogen. The second one implies the creation of oxygen vacancies in the ceria (ceria–zirconia) lattice, with inherent formation of water. Since this cannot be reversed by simple evacuation, it is referred to as irreversible [53]. Its contribution to the total reduction degree increases with T_{red} [53]. The distinction

between these two reduction processes is very relevant in order to fully understand the redox chemistry of these oxides. Also noteworthy is the drastic influence of Cl^- on the redox chemistry described above. In effect, as discussed in [37,53], in the presence of Cl^-, the reversible mechanism above becomes completely blocked. This is interpreted as due to the Cl^- incorporation into the ceria lattice [37].

3.2.1. Oxygen storage capacity (OSC) and related characterisation studies

Among the properties demanded of the redox materials by the TWC industry, the amount of oxygen that the material may exchange with the surrounding atmosphere, under certain pre-established conditions (temperature, chemical environment, and time of treatment), and the kinetics of these processes, are particularly relevant. Accordingly, a number of experimental techniques have been specifically developed for evaluating such properties. Oxygen storage capacity (OSC) constitutes the best example of these techniques [35,73,129–133]. Oxygen buffering capacity (OBC) may also be included in this category [134].

Regarding the oxygen storage capacity studies, ultimate [87,90,91,129,130] and dynamic [73,81,87,129,130, 133,135–139] OSC concepts are usually distinguished. The objective of the first type of OSC measurements is the evaluation of the highest amount of oxygen that may be extracted from the oxide, at a pre-established temperature and partial pressure of the reducing agent, usually H_2 or CO [130]. The OSC, i.e., the reduction degree reached by the sample, is usually determined by means of oxygen pulse techniques. Table 2 shows an example of an ultimate OSC study. It illustrates the influence of zirconia content on the oxygen storage capacity of a series of ceria–zirconia mixed oxides, including bare ceria. The results in table 2 are in qualitative agreement with those reported in [130], the highest OSC values being determined by the intermediate CeO_2/ZrO_2 molar ratios. However, in table 2, the differences from one oxide to the others are smaller. This may be interpreted as due to the applied reduction temperature, 673 K in [130], and 1273 K in table 2. Accordingly, ultimate OSC data are sensitive to the experimental conditions. This prevents the generalisation of conclusions drawn from OSC data obtained under certain specific conditions.

Dynamic OSC measurements are aimed at characterising the response of redox materials by alternately injecting H_2 (CO) and O_2 pulses. In this way, the amount of the most reactive oxygen species is considered to be evaluated [130]. The actual meaning of the recorded dynamic OSC data, however, deserves some analysis. In [133], a study on the dynamic OSC behaviour of a series of Rh-, Pd- and Pt-loaded ceria–zirconia, Pt/CeO_2, and Pt/Al_2O_3 catalysts is reported. Both H_2 and CO were used as reducing agents. Likewise, temperatures ranging from 298 to 773 K were investigated. Table 3 summarises some of the results reported in [133].

A first remarkable observation is the strong dependence of the OSC values in table 3 on the nature of the reducing agent. Likewise, the temperature at which OSC starts to be measurable is noticeably different. In effect, high H_2-OSC values are determined even at 298 K. As discussed in [133], this proves that the titration of the spilt over hydrogen may represent a major contribution to the H_2-OSC, which is certainly a relevant observation in relation to the chemical meaning of this parameter. The contribution of the spilt over hydrogen should be expected to decrease with the reduction temperature. Accordingly, at 773 K, H_2-OSC would mainly evaluate the actual oxygen exchange capability of the catalysts. Under these conditions, ceria–zirconia catalysts show a significantly better behaviour than those containing ceria.

The OBC technique also has a dynamic character. It allows us to quantitatively determine the capacity of a certain material for attenuating the oscillations induced on the oxygen partial pressure over it [134]. These oscillations are generated by fast (0.1 Hz) injection of O_2 (5%)/He pulses in a helium stream flowing through the reactor containing the sample. Because of the absence of any reducing agent, the information provided by this technique strictly accounts for the oxygen exchange capability of the investigated materials. This information is cer-

Table 2
Ultimate OSC study of a series of $Ce_xZr_{1-x}O_2$ mixed oxides

Oxide samples	S_{BET} ($m^2 \cdot g^{-1}$)[a]	OSC (mmole $O_2 \cdot g^{-1}$)	Ce^{3+} (%)
CeO_2	94	0.55	38
$Ce_{0.80}Zr_{0.20}O_2$	105	0.67	55
$Ce_{0.68}Zr_{0.32}O_2$	97	0.72	66
$Ce_{0.50}Zr_{0.50}O_2$	99	0.74	87
$Ce_{0.15}Zr_{0.85}O_2$	95	0.26	92

Oxides reduced at 1273 K (1 h), under flowing H_2 (5%)/Ar. Oxygen uptake measured at 700 K. Data taken from [91].
[a]BET surface of the starting (fresh) oxide samples.

Table 3
Dynamic OSC study of a series of Pt(Rh,Pd)/$Ce_{0.68}Zr_{0.32}O_2$, and Pt/CeO_2 catalysts. The experiments consisted of alternately pulsing H_2(CO) and O_2 every 70 s, for 30 min, at each of the selected temperatures

Catalyst sample[a]	S_{BET} ($m^2 \cdot g^{-1}$)	Reducing agent	Dynamic OSC (ml $O_2 \cdot g^{-1}_{catalyst}$)				
			298 K	373 K	473 K	573 K	773 K
Pt/$Ce_{0.68}Zr_{0.32}O_2$	100	H_2	6.3	7.1	7.5	7.6	8.9
Pt/$Ce_{0.68}Zr_{0.32}O_2$	21	H_2	1.5	2.0	4.4	5.0	6.8
Pd/$Ce_{0.68}Zr_{0.32}O_2$	85	H_2	6.2	7.1	7.4	7.7	8.8
Rh/$Ce_{0.68}Zr_{0.32}O_2$	94	H_2	2.4	6.5	7.7	8.0	9.0
Pt/CeO_2	88	H_2	4.2	4.5	4.4	3.6	3.4
Pt/CeO_2	18	H_2	1.4	1.6	1.5	1.3	1.3
$Ce_{0.68}Zr_{0.32}O_2$[b]	100	H_2	0.0	0.0	0.0	0.0	2.1
Pt/$Ce_{0.68}Zr_{0.32}O_2$	100	CO	–	0.7	1.7	2.3	2.4
Pd/$Ce_{0.68}Zr_{0.32}O_2$	85	CO	–	0.0	0.1	0.7	–
Rh/$Ce_{0.68}Zr_{0.32}O_2$	94	CO	–	0.0	0.1	8.6	–

Data taken from [133].
[a]Pre-treatment applied to the catalysts: Heating in a flow of (5%)H_2/Ar to 500 K (10 K min^{-1}), maintained at 500 K for 1 h, and cooled to 298 K always under flowing (5%)H_2/Ar. Finally, the samples were flushed with Ar for 30 min at 298 K.
[b]Pre-treatment applied to $Ce_{0.68}Zr_{0.32}O_2$: Heating in a flow of (5%)O_2/Ar to 823 K (10 K min^{-1}), for 1 h, cooling to 373 K in the same flow, and finally to 298 K under flowing Ar.

tainly of interest for better understanding fundamental aspects of the oxygen storage/release processes in TWCs.

3.2.2. *Temperature programmed reduction (TPR) studies*

TPR is probably the most commonly used technique for routine redox characterisation of ceria and ceria-based mixed oxides. Hydrogen is by far the most usual reducing agent [37]. Experiments have been performed under hydrogen partial pressures ranging from 760 Torr [140,141] to 7.6 Torr [84–86] [142–144]. Mass spectrometry (MS) and thermal conductivity detectors (TCD) have been used as analytical devices [37,73]. TCD detectors may only account for hydrogen consumption, whereas MS may provide simultaneous information on the evolution of both hydrogen (m/e = 2) and water (m/e = 18). This is a relevant difference because H_2 and H_2O traces may not be identical, as implicitly is assumed in the usual interpretation of the TPR–TCD diagrams [37,73]. This is particularly true in TPR studies on NM/CeO_2 (CeO_2–ZrO_2) catalyst. As already outlined, throughout a TPR experiment, two distinct, not necessarily coupled [73], processes may occur: Hydrogen chemisorption on the support, which is strongly favoured by the presence of highly dispersed noble metals (spillover), and creation of oxygen vacancies with inherent water evolution. TPR–TCD devices do not allow us to discriminate between these two contributions to the total hydrogen consumption. Moreover, MS may also detect the formation of CH_4 or CO resulting from the reduction of carbonate species often trapped in the bulk of these oxides [85,86,124]. Distortions in the TPR–TCD signal due to hydrogen consumption, but also to the formation of reduced species which cannot be retained by the trap located downstream of the reactor, may occur.

The TPR traces for high surface area ceria samples typically show two major features [5,73], the position of which shift towards lower temperatures as the H_2 pressure is increased [141]. As deduced from [73], under flowing H_2 (5%)/Ar, the first peak is observed at approximately 650 K, whereas the last one, much stronger, appears at approximately 1100 K.

The low temperature reduction peak is classically interpreted as due to a relatively fast surface process followed by a much slower diffusion of the oxygen vacancies into the bulk of the oxide [100]. This interpretation however, has been critically revised by Trovarelli *et al.* [75,145]. According to these authors, ceria reduction is not controlled by the diffusion step. Instead, differences in the thermodynamic properties of ceria microcrystals, as a function of their size, and the oxide sintering occurring during the experiment, are the key factors in determining the shape of the TPR diagram. As suggested by some other very recent TPR studies on CeO_2 [76] and CeO_2–ZrO_2 [76,146], this question is still a matter of debate.

TPR has been routinely used in comparative studies of OSC materials. Thus, the comparison of TPR traces for ceria and ceria–zirconia samples systematically shows that, in the latter case, the main reduction peak is shifted downwards by approximately 200 K [81,87]. This proves the strong effect of the ceria doping with zirconia on its reducibility.

TPR has also shown the different effect of redox cycling on the behaviour of high surface area (100 $m^2 \cdot g^{-1}$) ceria and ceria–zirconia ($Ce_{0.68}Zr_{0.32}O_2$) samples [87]. If successive cycles of reduction at 1273 K and re-oxidation to 700 K are applied to the fresh

oxides, the TPR traces for the resulting ceria samples show a deterioration in their reducibility, the low temperature feature in the fresh catalyst completely disappearing [5,18,75,86,87]. This contrasts with the behaviour observed for the ceria–zirconia sample. In spite of the loss of surface area occurred on cycling (20 $m^2 \cdot g^{-1}$), the position of the main reduction peak at 873 K is slightly shifted downwards, and a shoulder on the low temperature side of this peak is developed. We should conclude, accordingly, that the redox cycling treatments improve the reducibility of the mixed oxide. This is a rather general effect, which has also been reported for ceria–zirconia samples with other Ce/Zr molar ratios [91].

Some other very remarkable effects of the thermal ageing on the redox behaviour of the ceria–zirconia mixed oxides have also been revealed by TPR studies. Thus, it is presently known that the re-oxidation temperature used in the ageing cycles very much modifies the redox response of the resulting oxide [77,79,146]. As shown by the TPR diagrams for $Ce_{0.68}Zr_{0.32}O_2$ reported in [77], the mild re-oxidation treatment (MO), at 823 K, leads to a sample with much better reducibility than that exhibited by the one re-oxidised at 1223 K, high temperature re-oxidation treatment (HTO). Moreover, this effect is reversible, so that by alternating MO and HTO treatments after the corresponding TPR run, the main reduction peak shifts successively back (673 K) and forth (873 K) [77]. Figure 7 shows an example of the reversible changes induced on the reducibility of a $Ce_{0.5}Zr_{0.5}O_2$ by alternating MO and HTO cycles of redox ageing.

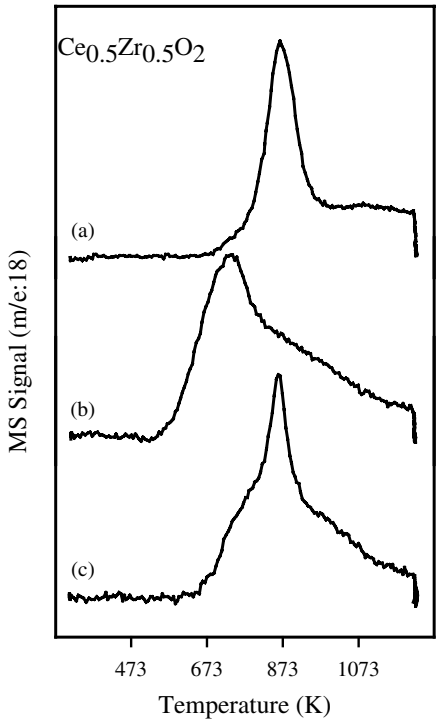

Figure 7. Reversibility of the changes induced on the TPR–MS diagram for a $Ce_{0.5}Zr_{0.5}O_2$ sample upon alternating HTO-1223 K (traces a and c) and MO-823 K (trace b) re-oxidation treatments in successive redox ageing cycles.

A number of factors seem to influence the observed instability of the redox properties of the ceria–zirconia mixed oxides. Among them, their textural properties [34], and the structural modifications occurring in their bulk [78–80,131,147,148] and/or their surface [146], might play a role. At present, however, this very intriguing behaviour is far from being fully understood.

Numerous TPR studies have proved the strong enhancing effect of the supported noble phases on the reducibility of ceria [5,35,73,149] and ceria zirconia mixed oxides [73]. This effect is usually interpreted as due to the low-temperature activation of H_2 on the metal, and its further transfer to the supports *via* a spillover mechanism. As already stressed in this work, this mechanism implies low temperature hydrogen consumption, but not necessarily simultaneous water formation [37,73]. Therefore, if oxide reduction is understood as lattice oxygen abstraction with inherent creation of vacancies, TPR–TCD experiments may overemphasise the actual enhancing effect of the supported metals on reducibility [73].

3.2.3. *Structural characterisation studies on OSC materials*

Numerous structural characterisation studies dealing with ceria–zirconia mixed oxides are presently available. X-ray [17,78,150–155] and neutron [156] diffraction, EXAFS [98,147,152,157,158], Raman spectroscopy [78,90,91,152,159], and HRTEM [159–162] are some of the applied experimental techniques.

The ceria–zirconia phase diagram shows that, as a function of the Ce/Zr molar ratio, monoclinic (molar percentage of Ce: 0–10), tetragonal (molar percentage of Ce: 10–80), and cubic (molar percentage of Ce: 80–100) phases may occur [18]. Consequent to the occurrence of some metastable tetragonal phases, the domain of compositions ranging from 10(Ce)/90(Zr) to 80(Ce)/20(Zr) molar ratios is particularly complex [18]. In general the tetragonal distortion observed in the mixed oxide phases, as determined by the (c/a) ratio, is lower than that found in pure zirconia, being dependent on the Ce content. Thus, for Ce/Zr molar ratios <(30/70), a tetragonal (*t*) phase, with c/a > 1, is observed. Also characteristic of the t form is that it may undergo the t → m (monoclinic) phase transition. For Ce/Zr ratios ranging from (30/70) to (65/35), a new phase (t′), with (c/a) close to 1, has been reported to occur. Finally, for the highest Ce/Zr ratios, a pseudo-cubic, t″ phase, with (c/a) = 1, but still showing an oxygen distorted structure along the *z* axis, is found. XRD, but also very important, Raman spectroscopy studies have provided

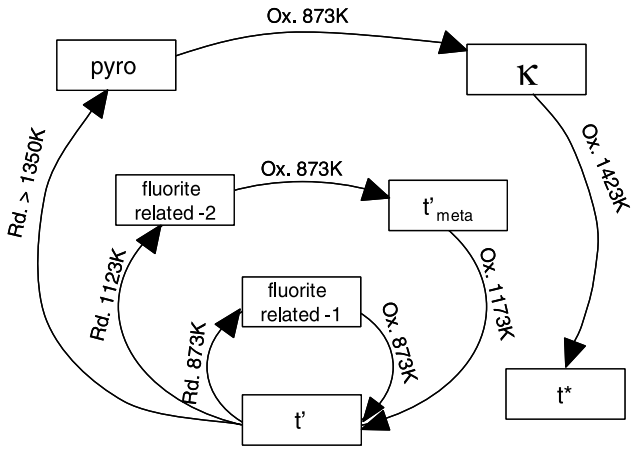

Figure 8. Structural evolution undergone by $Ce_{0.5}Zr_{0.5}O_2$ as a function of the applied redox ageing treatment. CaF_2 like and pyro, in the figure, stand respectively for defective fluorite-related-($Ce_{0.5}Zr_{0.5}O_{2-x}$), and pyrochlore ($Ce_{0.5}Zr_{0.5}O_{1.75}$) structures Scheme adapted from [78].

us with the experimental data for distinguishing t, t′, and t″ phases [18].

As deduced from the series of works on ceria–zirconia mixed oxides reported in [78–80,150,151,163], the main conclusions from which are summarised in figure 8, the structural behaviour of this system may be even more complex than that suggested above.

In accordance with figure 8 for intermediate Ce/Zr molar ratios, around (50/50), some additional phases, which are referred to as t'_{meta}, t*, and κ, may be formed. In the case of the κ-phase, the Rietveld analysis of its XRD pattern has allowed the assignment of its space group, $P2_13$ [150].

As shown in figure 8, the different structural forms are all prepared by applying to the starting t′ phase redox ageing cycles in which both the reduction and re-oxidation temperatures are varied [78]. In some cases, the observed structural changes are reversible, whereas, when a very high temperature reduction treatment is applied, the starting phase, t′, is not re-formed by the subsequent re-oxidation treatments. These structural changes would be related to the progressive ordering of the cationic sub-lattice as the reduction temperature is increased [78,150]. Accordingly, the cationic sub-lattice would evolve from a rather disordered situation in the t′ phase to a fully ordered state in the pyrochlore structure formed under very heavy reduction conditions. The re-oxidation treatments would induce the opposite effect, the intensity of which would depend on the applied temperature.

In parallel with the structural changes discussed above, noticeable modifications in the redox behaviour of the mixed oxides are observed [78–80]. In general samples prepared by high temperature reduction followed by re-oxidation at moderate temperatures, figure 8, lead to oxides exhibiting the best low-temperature reducibility [164]. These observations have suggested to the authors the existence of a close relationship between the bulk structural properties and the redox behaviour of these materials.

Though the cited research represents a significant advance in our knowledge, a comprehensive model integrating the rich variety of chemical and structural facts presently known is still lacking. Moreover, many of the applied ageing routines do not guarantee the structural homogeneity of the resulting mixed-oxide sample [160]. This introduces an additional difficulty in the interpretation of the structural data, and in the reproducibility of the structural and redox characterisation studies carried out on these materials. Likewise, the analysis of the results discussed in this section should take into account some recent studies [146]. In effect, it is suggested in [146] that the surface properties, rather than the bulk structure, would be particularly relevant in the control of the chemical (redox) reactivity of these oxides..

Acknowledgments

We acknowledge the financial support from MCYT (Project MAT 2002-2782), and the Junta de Andalucía. We are also indebted to Dr. C. Larese for her kind help during the elaboration of this work..

References

[1] K.C. Taylor, CHEMTECH (1990) 551.
[2] K.C. Taylor, in: *Frontiers of Materials Research/Electronic and Optical Materials*, eds. M. Kong and L. Huang (Elsevier, Amsterdam, 1991) p. 49–56.
[3] H. Muraki and G. Zhang, Catal. Today 63 (2000) 337.
[4] M. Shelef and R.W. McCabe, Catal. Today 62 (2000) 35.
[5] J. Kaspar, P. Fornasiero and N. Hickey, Catal. Today 77 (2003) 419.
[6] R.M. Heck and R.J. Farrauto, Appl. Catal. A: Gen. 221 (2001) 443.
[7] R.M. Heck, S. Gulati and R.J. Farrauto, Chem. Eng. J. 82 (2001) 149.
[8] R.M. Heck and R.J. Farrauto, *Catalytic Air Pollution Control: Commercial Technology* (Van Nostrand Reinhold, New York, 1995).
[9] H.C. Yao and Y.F. Yu Yao, J. Catal. 86 (1984) 254.
[10] E.S.J. Lox and B.H. Engler, in: *Handbook of Heterogeneous Catalysis*, eds. G. Ertl, H. Knözinger and J. Weitkamp Vol. 4,(VCH, Winheim, 1997) p. 1559–1633.
[11] P. Eastwood, *Crtitical Topics in Exhaust Gast Aftertreatment* (Research Studies Press Ltd, Baldock, 2000).
[12] M. Shelef, G.W. Graham and R.W. McCabe, in: *Catalysis, by Ceria and Related Materials*, ed. A. Trovarelli, (Imperial College Press, London, 2002) ch 10.
[13] R.J. Farrauto and R.M. Heck, Catal. Today 51 (1999) 351.
[14] H.S. Gandhi, G.W. Graham and R.W. McCabe, J. Catal. 216 (2003) 433.
[15] D.E. Webster, Top. Catal. 16/17 (2001) 33.
[16] J. Kaspar, M. Graziani and P. Fornasiero, in: *Handbook on the Physics and Chemistry of Rare Earths*, ed. K.A. Gschneidner and L. Eyring (Elsevier Science B.V., 2000) ch. 184.
[17] G. Colón, F. Valdivieso, M. Pijolat, R.T. Baker, J.J. Calvino and S. Bernal, Catal. Today 50 (1999) 271.

[18] J. Kaspar, P. Fornasiero and M. Graziani, Catal. Today 50 (1999) 285.
[19] A. Köning, G. Herding, B. Hupfeld, T. Richter and K. Weidmann, Top. Catal. 16/17 (2001) 23.
[20] H. Hirata, I. Hachisuka, Y. Ikeda, S. Tsuji and S. Matsumoto, Top. Catal. 16/17 (2001) 145.
[21] H. Shinjoh, N. Takahashi, K. Yokota and M. Sugiura, Appl. Catal. B: Environ. 15 (1998) 189.
[22] C. Larese, F. Cabello Galisteo, M. Lopez Granados, R. Mariscal, J.L.G. Fierro, M. Furió and R. Fernández-Ruiz, Appl. Catal. B: Environ. 40 (2003) 305.
[23] D.D. Beck, J.W. Sommers and C.L. DiMaggio, Appl. Catal. B: Environ. 11 (1997) 273.
[24] D.D. Beck, J.W. Sommers and C.L. DiMaggio, Appl. Catal. B: Environ. 11 (1997) 257.
[25] M.J. Rokosz, A.E. Chen, C.K. Lowe-Ma, A.V. Kucherov, D. Benson, M.C.P. Peck and R.W. McCabe, Appl. Catal. B: Environ. 33 (2001) 205.
[26] J.A. Moulijn, A.E. van Diepen and F. Kapteijn, Appl. Catal. A: Gen. 212 (2001) 3.
[27] C.H. Bartholomew, Appl. Catal. A: Gen. 212 (2001) 17.
[28] D.E. Angove and N.W. Cant, Catal. Today 63 (2000) 371.
[29] R. Fernández-Ruiz, M. Furio, F.C. Galisteo, C. Larese, M.L. Granados, R. Mariscal and J.L.G. Fierro, Anal. Chem. 74 (2002) 5463.
[30] M.A. Palacios, M.M. Gómez, M. Moldovan, G. Morrison, S. Rauch, C. McLeod, R. Ma, J. Laserna, P. Lucena, S. Caroli, A. Alimonti, F. Petrucci, B. Bocca, P. Schramel, S. Lustig, M. Zischka, U. Wass, B. Stenbom, M. Luna, J.C. Saenz, J. Santamaría and J.M. Torrens, Sci. Total Environ. 257 (2000) 1.
[31] D.E. Angove, N.W. Cant, D.H. French and K. Kinealy, Appl. Catal. A: Gen. 194/195 (2000) 27.
[32] A. Trovarelli (ed.), *Catalysis by Ceria and Related Materials*, (Imperial College Press, London, 2002).
[33] S. Bernal, J. Kaspar and A. Trovarelli (eds.), *Recent Progress in Catalysis by Ceria and Related Compounds*, Catal. Today 50 (1999) 173–443.
[34] J. Kaspar and P. Fornasiero, J. Solid State Chem. 171 (2003) 19.
[35] A. Trovarelli, Catal. Rev. Sci. Eng. 38 (1996) 439.
[36] S. Bernal, J.J. Calvino, M.A. Cauqui, J.M. Gatica, C. Larese, J.A. Pérez-Omil and J.M. Pintado, Catal. Today 50 (1999) 175.
[37] S. Bernal, J.J. Calvino, J.M. Gatica, C. López-Cartes and J.M. Pintado, in: *Catalysis by Ceria and Related Materials*, ed., A. Trovarelli (Imperial College Press, London, 2002) ch. 4.
[38] S. Bernal, J.J. Calvino, M.A. Cauqui, J.A. Pérez-Omil, J.M. Pintado and J.M. Rodríguez-Izquierdo, Appl. Catal. B: Environ. 16 (1998) 127.
[39] S. Bernal, F.J. Botana, J.J. Calvino, C. López-Cartes, J.A. Pérez-Omil and J.M. Rodríguez-Izquierdo, Ultramicroscopy 72 (1998) 135.
[40] J.M. Gatica, R.T. Baker, P. Fornasiero, S. Bernal, G. Blanco and J. Kaspar, J. Phys. Chem. B 104 (2000) 4667.
[41] J.M. Gatica, R.T. Baker, P. Fornasiero, S. Bernal and J. Kaspar, J. Phys. Chem. B 105 (2001) 1191.
[42] A.K. Datye, D. Kalakkad, M.H. Yao and D.J. Smith, J. Catal. 155 (1995) 148.
[43] L. Kepinski and M. Wolcyrz, Appl. Catal. A: Gen. 150 (1997) 197.
[44] M. Pan, J.M. Cowley and R. García, Micron Microsc. Acta 18 (1987) 165.
[45] S. Bernal, F.J. Botana, J.J. Calvino, G.A. Cifredo, J.A. Pérez-Omil and J.M. Pintado, Catal. Today 28 (1995) 219.
[46] S. Bernal, J.J. Calvino, J.M. Gatica, C. Larese, C. López-Cartes and J.A. Pérez-Omil, J. Catal. 169 (1997) 510.
[47] S. Bernal, J.J. Calvino, M.A. Cauqui, J.M. Gatica, C. Lopez Cartes, J.A. Perez Omil and J.M. Pintado, Catal. Today 77 (2003) 385.
[48] L. Kepinski, M. Wolcyrz and J. Okal, J. Chem. Soc., Faraday Trans. 91 (1995) 507.
[49] S. Bernal, G. Blanco, J.J. Calvino, C. López-Cartes, J.A. Pérez-Omil, J.M. Gatica, O. Stephan and C. Colliex, Catal. Lett. 76 (2001) 131.
[50] S. Bernal, J.J. Calvino, J.M. Gatica, C. López-Cartes and J.M. Pintado, in: *Catalysis by Ceria and Related Materials*, ed. A. Trovarelli (Imperial College Press, London, 2002) ch. 4.
[51] S. Bernal, J.J. Calvino, G.A. Cifredo, J.M. Rodríguez-Izquierdo, V. Perrichon and A. Laachir, J. Chem. Soc., Chem. Commun. (1992) 460.
[52] S. Bernal, J.J. Calvino, G.A. Cifredo, J.M. Rodríguez-Izquierdo, V. Perrichon and A. Laachir, J. Catal. 137 (1992) 1.
[53] S. Bernal, J.J. Calvino, G.A. Cifredo and J.M. Rodríguez-Izquierdo, J. Phys. Chem. 99 (1995) 11794.
[54] A. Bensalem, F. Bozon-Verduraz and V. Perrichon, J. Chem. Soc., Faraday Trans. 91 (1995) 2185.
[55] A. Norman, V. Perrichon, A. Bensaddik, S. Lemaux, H. Bitter and D.C. Koningsberger, Top. Catal. 16/17 (2001) 363.
[56] S. Bernal, F.J. Botana, J.J. Calvino, M.A. Cauqui, G.A. Cifredo, A. Jobacho, J.M. Pintado and J.M. Rodríguez-Izquierdo, J. Phys. Chem. 97 (1993) 4118.
[57] S. Bernal, J.J. Calvino, M.A. Cauqui, G.A. Cifredo, A. Jobacho and J.M. Rodríguez-Izquierdo, Appl. Catal. 99 (1993) 1.
[58] P. Fornasiero, J. Kaspar and M. Graziani, J. Catal. 167 (1997) 576.
[59] C. Force, J.P. Belzunegui, J. Sanz, A. Martinez-Arias and J. Soria, J. Catal. 197 (2001) 192.
[60] C. Li, Y. Sakata, T. Arai, K. Domen, K. Maruya and T. Onishi, J. Chem. Soc., Faraday Trans. 85 (1989) 1451.
[61] D.W. Daniel, J. Phys. Chem. 92 (1988) 3891.
[62] M. Primet, M. El Azhar, R. Frety and M. Guenin, Appl. Catal. 59 (1990) 153.
[63] A. Bensalem, J.C. Muller, D. Tessier and F. Bozon-Verduraz, J. Chem. Soc., Faraday Trans. 92 (1996) 3233.
[64] C. Binet, A. Jadi, J.C. Lavalley and M. Boutonnet-Kizling, J. Chem. Soc., Faraday Trans. 88 (1992) 2079.
[65] J. Cunningham, D. Cullinane, J. Sanz, J.M. Rojo, J. Soria and J.L.G. Fierro, J. Chem. Soc., Faraday Trans. 88 (1992) 3233.
[66] A. Badri, C. Binet and J.C. Lavalley, J. Phys. Chem. 100 (1996) 8363.
[67] D.I. Kondarides and X.E. Verykios, J. Catal. 174 (1998) 52.
[68] J.L. Duplan and H. Praliaud, Appl. Catal. 67 (1991) 325.
[69] A. Holmgren and B. Andersson, J. Catal. 178 (1998) 14.
[70] S. Bernal, G. Blanco, J.M. Gatica, C. Larese and H. Vidal, J. Catal. 200 (2001) 411.
[71] P. Meriaudeau, J.F. Dutel, M. Dufaux and C. Naccache, Metal-Supp. Metal-Add. Eff. Catal. (1982) 95.
[72] A. Badri, C. Binet and J.C. Lavalley, J. Chem. Soc., Faraday Trans. 92 (1996) 1603.
[73] M. Boaro, M. Vicario, C. de Leitenburg, G. Dolcetti and A. Trovarelli, Catal. Today 77 (2003) 407.
[74] E. Rocchini, M. Vicario, J. Llorca, C. de Leitenburg, G. Dolcetti and A. Trovarelli, J. Catal. 211 (2002) 407.
[75] F. Giordano, A. Trovarelli, C. de Leitenburg and M. Giona, J. Catal. 193 (2000) 273.
[76] P. Fornasiero, J. Kaspar and M. Graziani, Appl. Catal. B: Environ. 22 (1999) L11.
[77] R.T. Baker, S. Bernal, G. Blanco, A.M. Cordon, J.M. Pintado, J.M. Rodriguez-Izquierdo, F. Fally and V. Perrichon, Chem. Commun. (1999) 149.
[78] N. Izu, H. Kishimoto, T. Omata, K. Ono and S. Otsuka-Yao-Matsuo, Sci. Technol. Adv. Mater. 2 (2001) 397.
[79] S. Otsuka-Yao-Matsuo, T. Omata, N. Izu and H. Kishimoto, J. Solid State Chem. 138 (1998) 47.
[80] N. Izu, T. Omata and S. Otsuka-Yao-Matsuo, J. Alloys Compd. 270 (1998) 107.
[81] C.E. Hori, A. Brenner, K.Y. Simon Ng, K.M. Rahmoeller and D. Belton, Catal. Today 50 (1999) 299.

[82] P. Fornasiero, G. Balducci, R. di Monte, J. Kaspar, V. Sergo, G. Gubitosa, A. Ferrero and M. Graziani, J. Catal. 164 (1996) 173.
[83] G. Balducci, P. Fornasiero, R. di Monte, J. Kaspar, S. Meriani and M. Graziani, Catal. Lett. 33 (1995) 193.
[84] V. Perrichon, A. Laachir, G. Bergeret, R. Frety, L. Tournayan and O. Touret, J. Chem. Soc., Faraday Trans. 90 (1994) 773.
[85] F.M.Z. Zotin, L. Tournayan, J. Varloud, V. Perrichon and R. Frety, Appl. Catal. 98 (1993) 99.
[86] A. Laachir, V. Perrichon, A. Badri, J. Lamotte, E. Catherine, J.C. Lavalley, J. El Fallah, L. Hilaire, F. Le Normand, E. Quéméré, G.N. Sauvion and O. Touret, J. Chem. Soc., Faraday Trans. 87 (1991) 1601.
[87] F. Fally, V. Perrichon, H. Vidal, J. Kaspar, M. Daturi, J.C. Lavalley, G. Blanco, J.M. Pintado and S. Bernal, Catal. Today 59 (2000) 387.
[88] S. Bernal, G. Blanco, J.J. Calvino, G.A. Cifredo, J.A. Pérez-Omil, J.M. Pintado and A. Varo, Stud. Surf. Sci. Catal. 82 (1994) 507.
[89] H. Vidal, S. Bernal, J. Kaspar, M. Pijolat, V. Perrichon, G. Blanco, J.M. Pintado, R.T. Baker, G. Colon and F. Fally, Catal. Today 54 (1999) 93.
[90] H. Vidal, J. Kaspar, M. Pijolat, G. Colón, S. Bernal, A.M. Cordón, V. Perrichon and F. Fally, Appl. Catal. B: Environ. 30 (2001) 75.
[91] H. Vidal, J. Kaspar, M. Pijolat, G. Colón, S. Bernal, A.M. Cordón, V. Perrichon and F. Fally, Appl. Catal. B: Environ. 27 (2000) 49.
[92] M. Daturi, E. Finocchio, C. Binet, J.C. Lavalley, F. Fally and V. Perrichon, J. Phys. Chem. B 103 (1999) 4884.
[93] S. Salasc, V. Perrichon, M. Primet, M. Chevrier, F. Mathis and N. Moral, Catal. Today 50 (1999) 227.
[94] S. Bernal, J.J. Calvino, G.A. Cifredo, J.M. Gatica, J.A. Pérez-Omil, A. Laachir and V. Perrichon, Stud. Surf. Sci. Catal. 96 (1995) 419.
[95] A. Laachir, V. Perrichon, S. Bernal, J.J. Calvino and G.A. Cifredo, J. Mol. Catal. 89 (1994) 391.
[96] A. Badri, J. Lamotte, J.C. Lavalley, A. Laachir, V. Perrichon, O. Touret, G.N. Sauvion and E. Quéméré, Eur. J. Solid State Inorg. Chem. 28 (1991) 445.
[97] D.R. Mullins, S.H. Overbury and D.R. Huntley, Surf. Sci. 409 (1998) 307.
[98] J.A. Rodríguez, J.C. Hanson, J.Y. Kim, G. Liu, A.I. Juez and M.F. García, J. Phys. Chem. B 107 (2003) 3535.
[99] J.C. Conesa, M. Fernández-García and A. Martínez-Arias, in: *Catalysis by Ceria and Related Materials*, ed. A. Trovarelli (Imperial College Press, London, 2002) ch. 5.
[100] J. El Fallah, S. Boujana, H. Dexpert, A. Kiennemann, J. Majerus, O. Touret, F. Villain and F. Le Normand, J. Phys. Chem. 98 (1994) 5522.
[101] F. Le Normand, L. Hilaire, K. Kili, G. Krill and G. Maire, J. Phys. Chem. 92 (1988) 2561.
[102] C. López-Cartes, S. Bernal, J.J. Calvino, M.A. Cauqui, G. Blanco, J.A. Pérez-Omil, J.M. Pintado, S. Helveg and P.L. Hansen, Chem. Commun. (2003) 644.
[103] R. Sharma, Microsc. Microanal. 7 (2001) 494.
[104] L.A.J. Garvie and P.R. Buseck, J. Phys. Chem. Solids 60 (1999) 1943.
[105] J.P. Holgado, R. Alvarez and G. Munuera, Appl. Surf. Sci. 161 (2000) 301.
[106] J.P. Holgado, G. Munuera, J.P. Espinos and A.R. Gonzalez-Elipe, Appl. Surf. Sci. 158 (2000) 164.
[107] M.Y. Sinev, G.W. Graham, L.P. Haack and M. Shelef, J. Mater. Res. 11 (1996) 1960.
[108] S. Bernal, G. Blanco, M.A. Cauqui, A.I. Martin, J.M. Pintado, A. Galtayries and R. Sporken, Surf. Interf. Anal. 30 (2000) 85.
[109] M. Daturi, C. Binet, J.C. Lavalley, A. Galtayries and R. Sporken, Phys. Chem. Chem. Phys. 1 (1999) 5717.
[110] S.H. Overbury, D.R. Mullins, D.R. Huntley and Lj. Kundakovic, J. Catal. 186 (1999) 296.
[111] D.I. Kondarides and X.E. Verykios, J. Catal. 174 (1998) 52.
[112] A. Galtayries, R. Sporken, G. Blanchard and R. Caudano, J. Electron Spectrosc. Relat. Phenom. 88–91 (1998) 951.
[113] A. Pfau, J. Sanz, K.D. Schierbaum, W. Göpel, J.P. Belzunegui and J.M. Rojo, Stud. Surf. Sci. Catal. 101 (1996) 931.
[114] A. Pfau, K.D. Schierbaum and W. Göpel, Surf. Sci. 331–333 (1995) 1479.
[115] Y. Zhou, M. Nakashima and J.M. White, J. Phys. Chem. 92 (1988) 812.
[116] T. Jin, Y. Zhou, G.J. Mains and J.M. White, J. Phys. Chem. 91 (1987) 5931.
[117] M. Fernandez-Garcia, A. Martinez-Arias, A. Iglesias-Juez, A.B. Hungria, J.A. Anderson, J.C. Conesa and J. Soria, Appl. Catal. B: Environ. 31 (2001) 39.
[118] A. Martinez-Arias, M. Fernandez-Garcia, A. Iglesias-Juez, A.B. Hungria, J.A. Anderson, J.C. Conesa and J. Soria, Appl. Catal. B: Environ. 31 (2001) 51.
[119] M. Fernández-García, A. Martinez-Arias, A. Iglesias-Juez, C. Belver, A.B. Hungria, J.C. Conesa and J. Soria, J. Catal. 194 (2000) 385.
[120] A. Martinez-Arias, M. Fernández-García, J. Soria and J.C. Conesa, J. Catal. 182 (1999) 367.
[121] A. Martínez-Arias, J. Soria and J.C. Conesa, J. Catal. 168 (1997) 364.
[122] M. Daturi, E. Finocchio, C. Binet, J.C. Lavalley, F. Fally, V. Perrichon, H. Vidal, J.N. Hickey and J. Kaspar, J. Phys. Chem. B 104 (2000) 9186.
[123] C. Binet, M. Daturi and J.C. Lavalley, Catal. Today 50 (1999) 207.
[124] C. Binet, A. Badri and J.C. Lavalley, J. Phys. Chem. 98 (1994) 6392.
[125] C. Binet, A. Badri, M. Boutonnet-Kizling and J.C. Lavalley, J. Chem. Soc., Faraday Trans. 90 (1994) 1023.
[126] C. Binet, A. Jadi and J.C. Lavalley, J. Chim. Phys. 88 (1991) 499.
[127] S. Bernal, J.J. Calvino, G.A. Cifredo, A. Laachir, V. Perrichon and J.M. Herrmann, Langmuir 10 (1994) 717.
[128] J.M. Herrmann, E. Ramaroson, J.F. Tempere and M.F. Guilleux, Appl. Catal. 53 (1989) 117.
[129] S. Bedrane, C. Descorme and D. Duprez, Catal. Today 73 (2002) 233.
[130] D. Duprez and C. Descorme, in: *Catalysis by Ceria and Related Materials*, A. Trovarelli (Imperial College Press, London, 2002) ch. 7.
[131] A. Trovarelli, M. Boaro, E. Rocchini, C. de Leitenburg and G. Dolcetti, J. Alloys Compd. 323/324 (2001) 584.
[132] D. Terribile, J. Llorca, M. Boaro, C. de Leitenburg, G. Dolcetti and A. Trovarelli, Chem. Commun. (1998) 1897.
[133] N. Hickey, P. Fornasiero, J. Kaspar, J.M. Gatica and S. Bernal, J. Catal. 200 (2001) 181.
[134] S. Bernal, G. Blanco, M.A. Cauqui, P. Corchado, J.M. Pintado and J.M. Rodriguez-Izquierdo, Chem. Commun. (1997) 1545.
[135] Y. Sakamoto, K. Kizaki, T. Motohiro, Y. Yokota, H. Sobukawa, M. Uenishi, H. Tanaka and M. Sugiura, J. Catal. 211 (2002) 157.
[136] N. Hickey, P. Fornasiero, R. Di Monte, J. Kaspar, M. Graziani and G. Dolcetti, Catal. Lett. 72 (2001) 45.
[137] S. Bedrane, C. Descorme and D. Duprez, Catal. Today 75 (2002) 401.
[138] M. Boaro, C. Leitenburg, G. Dolcetti and A. Trovarelli, J. Catal. 193 (2000) 338.
[139] N. Hickey, P. Fornasiero, J. Kaspar, M. Graziani, G. Blanco and S. Bernal, Chem. Commun. (2000) 357.
[140] S. Bernal, F.J. Botana, R. García, F. Ramírez and J.M. Rodríguez-Izquierdo, Mater. Chem. Phys. 18 (1987) 119.
[141] S. Bernal, J.J. Calvino, G.A. Cifredo, J.M. Gatica, J.A. Pérez-Omil and J.M. Pintado, J. Chem. Soc., Faraday Trans. 89 (1993) 3499.

[142] A. Laachir, V. Perrichon, A. Badri, J. Lamotte, E. Catherine, J.C. Lavalley, J. El Fallah, L. Hilaire, F. Le Normand, E. Quéméré, G.N. Sauvion and O. Touret, J. Chem. Soc., Faraday Trans. 87 (1991) 1601.
[143] F.M.Z. Zotin, L. Tournayan, J. Varloud, V. Perrichon and R. Frety, Appl. Catal. 98 (1993) 99.
[144] V. Perrichon, A. Laachir, G. Bergeret, R. Frety, L. Tournayan and O. Touret, J. Chem. Soc., Faraday Trans. 90 (1994) 773.
[145] F. Giordano, A. Trovarelli, C. de Leitenburg, G. Dolcetti and M. Giona, Ind. Eng. Chem. Res. 40 (2001) 4828.
[146] P. Fornasiero, T. Montini, M. Graziani, J. Kaspar, A.B. Hungría, A. Martínez-Arias and J.C. Conesa, Phys. Chem. Chem. Phys. 4 (2002) 149.
[147] S. Lemaux, A. Bensaddik, A.M.J. van der Eerden, J.H. Bitter and D.C. Koningsberger, J. Phys. Chem. B 105 (2001) 4810.
[148] P. Fornasiero, E. Fonda, R. Di Monte, G. Vlaic, J. Kaspar and M. Graziani, J. Catal. 187 (1999) 177.
[149] C. Leitenburg, A. Trovarelli and J. Kaspar, J. Catal. 166 (1997) 98.
[150] H. Kishimoto, T. Omata, S. Otsuka-Yao-Matsuo, K. Ueda, H. Hosono and H. Kawazoe, J. Alloys Compd. 312 (2000) 94.
[151] S. Otsuka-Yao-Matsuo, N. Izu, T. Omata and K. Ikeda, J. Electrochem. Soc. 145 (1998) 1406.
[152] G. Vlaic, R. di Monte, P. Fornasiero, E. Fonda, J. Kaspar and M. Graziani, J. Catal. 182 (1999) 378.
[153] M. Yashima, K. Morimoto, N. Ishizawa and M. Yoshimura, J. Am. Ceram. Soc. 76 (1993) 1745.
[154] M. Yashima, K. Morimoto, N. Ishizawa and M. Yoshimura, J. Am. Ceram. Soc. 76 (1993) 2865.
[155] H.Y. Zhu, J. Am. Ceram. Soc. 77 (1994) 2458.
[156] S. Enzo, F. Delogu, R. Frattini, A. Primavera and A. Trovarelli, J. Mater. Res. 15 (2000) 1538.
[157] Y. Nagai, T. Yamamoto, T. Tanaka, S. Yoshida, T. Nonaka, T. Okamoto, A. Suda and M. Sugiura, Catal. Today 74 (2002) 225.
[158] G. Vlaic, P. Fornasiero, S. Geremia, J. Kaspar and M. Graziani, J. Catal. 168 (1997) 386.
[159] G. Colón, M. Pijolat, F. Valdivieso, H. Vidal, J. Kaspar, E. Finocchio, M. Daturi, C. Binet, J.C. Lavalley, R.T. Baker and S. Bernal, J. Chem. Soc., Faraday Trans. 94 (1998) 3717.
[160] T. Masui, T. Ozaki, G. Adachi, Z. Kang and L. Eyring, Chem. Lett. (2000) 840.
[161] H. Vidal, S. Bernal, J. Kaspar, M. Pijolat, V. Perrichon, G. Blanco, J.M. Pintado, R.T. Baker, G. Colón and F. Fally, Catal. Today 54 (1999) 93.
[162] R.T. Baker, S. Bernal, C. López-Cartes, J.A. Pérez-Omil and Y. Montardi, Inst. Phys. Conf. Ser. 161 (1999) 521.
[163] T. Omata, H. Kishimoto, S. Otsuka-Yao-Matsuo, N. Ohtori and N. Umesaki, J. Solid State Chem. 147 (1999) 573.
[164] G. Colón, M. Pijolat, F. Valdivieso, R.T. Baker and S. Bernal, Adv. Sci. Technol. Ser. 16 (1999) 605.